Water-Induced Interactions between Carbon Nanoparticles

Liwei Li, Dmitry Bedrov, and Grant D. Smith*

Department of Materials Science and Engineering and Department of Chemical Engineering, University of Utah, Salt Lake City, Utah 84112

Received: February 2, 2006; In Final Form: March 27, 2006

Molecular dynamics simulations were carried out in order to study the hydration of C_{60} fullerenes, carbon nanotubes, and graphene sheets in aqueous solution and the nature of water-induced interactions between these carbon nanoparticles. The hydration of these nonpolar carbon nanoparticles does not exhibit classical hydrophobic character due to the high density of surface atoms (carbon) resulting in strong water−surface dispersion interactions. Water was found to wet the nanoparticle surfaces independent of nanoparticle surface curvature, with the decrease in the extent of water−water hydrogen bonding with decreasing surface curvature being offset by stronger water−surface interactions. While all carbon nanoparticles investigated are anticipated to aggregate in water due to strong direct nanoparticle−nanoparticle interactions, the water-induced interactions between nanoparticles were found to be repulsive and, in contrast to the wetting behavior, were observed to exhibit strong dependence on surface curvature. The strength of the water-induced interaction between carbon nanoparticles was found to correlate well with the number of hydration water molecules displaced upon particle aggregation, which, relative to the amount of direct nanoparticle−nanoparticle contact engendered upon aggregation, decreases with decreasing surface curvature.

I. Introduction

Understanding how carbon-based nanoparticles such as fullerenes, nanotubes, and graphene sheets interact with biological systems as well as the ability to control their self-association behavior in aqueous environments requires fundamental understanding of how these nanoparticles interact with water and how water influences interaction between nanoparticles. Our recent molecular dynamics (MD) simulation studies of C_{60} fullerenes in water[1,2] illustrated that their association is dominated by strong direct fullerene−fullerene attractive interactions. Surprisingly, water-induced interactions between the fullerenes were found to be repulsive. Specifically, it was found that the high atomic density on the fullerene surface gives rise to highly favorable water−fullerene interactions due to strong carbon−water dispersion interactions. The energetic origin of this water-induced repulsive interaction between the carbon nanoparticles is in stark contrast to the entropy-driven association observed for conventional hydrophobic nonpolar organic solutes.[3,4] In this work we extend our MD simulation studies of the hydration and water-induced interactions between carbon-based nanoparticles to single-walled carbon nanotubes and graphene sheets.

II. Systems and Methodology

A. Systems. MD simulations were performed on one and two carbon-based nanoparticles (C_{60} fullerenes, carbon nanotubes, and graphene sheets) in aqueous solution at 298 K. The sizes of nanoparticles N_{carbon} as well as the number of water molecules N_{water} in the two nanoparticle systems are summarized in Table 1. The dimensions of the simulation cells are also given in Table 1. A full description of the C_{60} fullerene simulation system, illustrated in Figure 1a, can be found in our previous papers.[1,2] Parallel single-walled carbon nanotubes CNT(5,5)s and CNT-(16,0)s, denoted as CNT-1 and CNT-2, respectively, as illustrated in Figure 1b and 1c, were periodic in one dimension. The parallel graphene sheets, illustrated in Figure 1d, were periodic in two dimensions. To maintain mechanical and chemical equilibrium between water molecules between and outside of the two graphene sheets as the separation between graphene sheets was changed, a small region (35 carbon atoms) of each graphene was made permeable to water as illustrated in Figure 1e. The permeable region, which has no interaction with water molecules, accounts for 3.6% of the total graphene surface area.

The intermolecular four point potential (TIP4P) model[5] was employed to represent water molecules. Nonbonded interactions between carbon atoms and between carbon atoms and water were described by Lennard-Jones potentials of the form

$$U_{ij}(R_{ij}) = 4\epsilon_{ij}\left[\left(\frac{\sigma_{ij}}{R_{ij}}\right)^{12} - \left(\frac{\sigma_{ij}}{R_{ij}}\right)^{6}\right] \quad (1)$$

where R_{ij} is the separation between atoms i and j. The carbon−carbon nonbonded interaction parameters ($\sigma_{CC} = 3.47$ Å, $\epsilon_{CC} = 0.0660$ kcal mol^{-1}) were found to reproduce experimentally measured C_{60} crystal properties[6] and have been used extensively in C_{60} simulations.[7−10] The carbon−water interaction parameters ($\sigma_{CO} = 3.19$ Å, $\epsilon_{CO} = 0.0936$ kcal mol^{-1}) were adopted by Werder et al.[11] to reproduce the macroscopic contact angle of a water droplet on a graphite sheet. To better understand the role of carbon−water dispersion interactions on the interaction of water with carbon nanoparticles, we carried out additional simulations utilizing a Weeks−Chandler−Anderson (WCA)[12] interaction between water and carbon given as

$$U_{CO}^{WCA}(R_{ij}) = 4\epsilon_{ij}\left[\left(\frac{\sigma_{ij}}{R_{ij}}\right)^{12} - \left(\frac{\sigma_{ij}}{R_{ij}}\right)^{6} + 0.25\right] \quad \text{for } R_{ij} \le \sqrt[6]{2}\sigma_{ij} \quad (2)$$

$$U_{CO}^{WCA}(R_{ij}) = 0 \text{ otherwise}$$

10.1021/jp060718m CCC: $33.50
Published on Web 05/05/2006

TABLE 1: System Parameters

solute	N_{carbon}	N_{water}	D_s (Å)	cell dimension $(x\times y\times z)^a$ (Å^3)	ρ_{shell}(Å^{-3})	$N_{water,shell}$
C_{60}	60	1500	10.02	30.000 × 30.000 × 51.575	0.041	0.948
CNT-1	240	1300	10.06	50.515 × 29.569 × 29.528	0.044	0.493
CNT-2	448	1500	15.90	55.780 × 34.428 × 29.960	0.044	0.382
graphene	960	3000	3.46	52.050 × 50.070 × 42.455	0.045	0.248

[a] Average cell dimension at a solute surface separation of 6.0 Å.

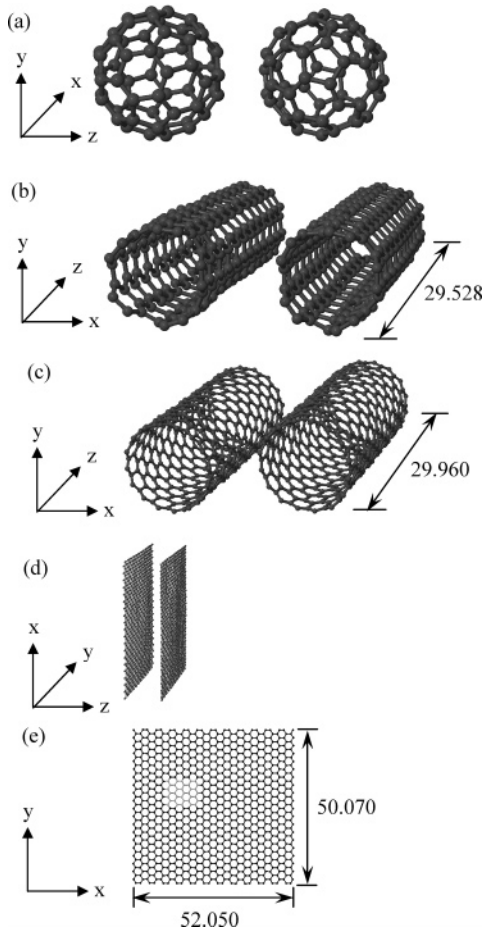

Figure 1. Carbon nanoparticles employed in the simulation studies. (a) C_{60} fullerenes, (b) CNT-1, (c) CNT-2, (d) graphenes, (e) structure of a graphene sheet showing carbon atoms (light gray) not visible to water molecules.

This interaction is purely repulsive and is often used to represent the interaction of hydrophobic solutes with water.[13] Cosine angle bends ($\theta = 120.0°$, $K_\theta = 134.4$ kcal mol^{-1}) and a 2-fold torsion ($K_\varphi = 6.0$ kcal mol^{-1}) were used in CNTs and graphenes modeling.[14]

B. Molecular Dynamics Simulations. MD simulations were carried out using the simulation package Lucretius.[15] The SHAKE algorithm[16] was employed to constrain bond lengths. The C_{60} fullerenes were made completely rigid by applying 120 additional bond constraints to each fullerene molecule. Nearly-rigid shapes of the CNTs and graphene sheets were maintained by adding additional bond constraints to the CNTs (110 to CNT-1 and 208 to CNT-2) and applying large "out-of-plane deformation" force constant to the graphene sheets (1500 kcal mol^{-1} rad^{-2}). The particle mesh Ewald algorithm[17] was used to treat the long-range water−water electrostatic interactions. Lennard-Jones interactions and electrostatic interactions in real space were truncated at 10 Å. In the graphene systems, the pressure, forces, and potential energy were corrected for anisotropic density profiles normal to the graphene sheets.[18] Simulations were run in orthorhombic cells subject to periodic boundary conditions in all spatial dimensions. The length of CNTs and the dimensions of the graphene sheets (surface area) were fixed while the remaining cell dimensions, specifically the x and y dimensions for the CNT and the z dimension for the graphene systems (illustrated in Figure 1) were subjected to isothermal−isobaric constraints to maintain a pressure (normal stress) of 1 atm in these directions. Simulations for C_{60} fullerene systems were run in the NVT ensemble where simulation box size was determined to yield 1 atm pressure for far-separated configurations of the fullerenes as described in our previous papers.[1,2] The Nosé−Hoover thermostat[19,20] was implemented to maintain system temperature of 298 K and Anderson−Hoover barostat,[20,21] which was adapted to accommodate orthorhombic simulation cell, was used in pressure control. The equations of motion were integrated by employing a multiple time step reversible reference system propagator algorithm.[22]

Determination of the potential of mean force (PMF) as a function of fullerene separation is described in detail in our previous work.[1,2] For CNTs and graphene sheets, the nanoparticles were constrained to a series of fixed center-of-mass separations and the PMF was obtained by integrating the average constraining force. The CNT and graphene separation was sampled from contact to a 10 Å surface separation in 0.2 Å increments. Obtaining accurate average forces requires 2 ns of simulation for each separation.

III. Structure of Hydrating Water

The water density profile $\rho(r)/\rho_{bulk}$ is shown in the main panel of Figure 2a for repulsive nanoparticle−water interactions (eq 2) and of Figure 2b for realistic (Lennard-Jones) nanoparticle−water interactions (eq 1). The profile is measured relative to the surface of the nanoparticle whose diameter (C_{60}, CNT) or thickness (graphene) D_s is given in Table 1. The size of the nanoparticle is given by the center-of-mass separation of the nanoparticle pairs at which the PMF in vacuum was most attractive (see section IV). The PMF between water and the nanoparticle, or equivalently the free energy $A(r)$ as a function of water−nanoparticle separation, also shown in insets of Figure 2, is given as

$$A(r) = -k_B T \ln \frac{\rho(r)}{\rho_{bulk}} \qquad (3)$$

where k_B is the Boltzmann constant, T is temperature and ρ_{bulk} is the density of water far from the nanoparticle surface (0.033 water molecules per Å^3). Figures 3a and 3b show the number of hydrogen bonds a water molecule forms with other water molecules as a function of separation for the nanoparticle surface for repulsive and realistic nanoparticle−water interactions, respectively. Here, a hydrogen bond between water molecules considered formed when the O···O distance is less than 3.4 Å and the O−H···O angle is less than 30°.

A. Repulsive Carbon Nanoparticle−Water Interactions. When water−nanoparticle interactions are repulsive, the density

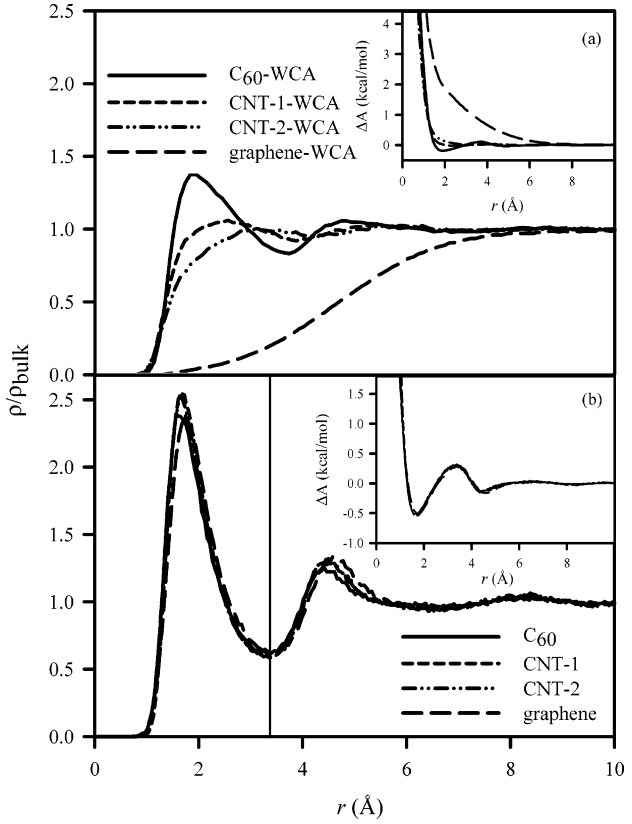

Figure 2. Water density profile (main panel) and the corresponding water free energy profile (inset) as a function of distance from a carbon nanoparticle surface for (a) water−carbon WCA potential and (b) realistic water−carbon Lennard-Jones potential. Here *r* is measured from the surface of nanoparticle to the oxygen atom of the water molecule. The vertical solid line in panel (b) indicates the boundary of the first hydration shell.

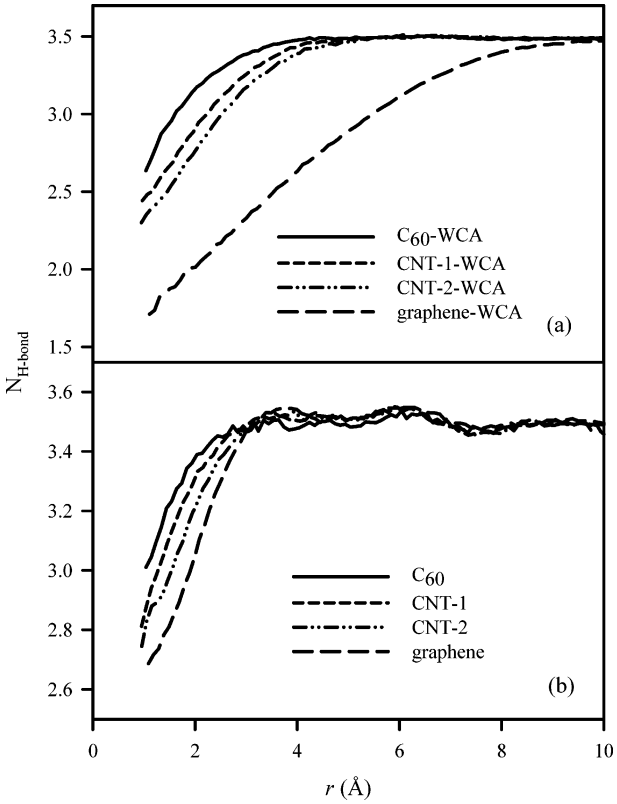

Figure 3. Hydrogen bonds per water with (a) WCA water−solute potential and (b) realistic water−solute Lennard-Jones potential. Here *r* is measured from the surface of nanoparticle to the oxygen atom of the water molecule.

and hydrogen bonding profiles reveal that the structure of water hydrating the nanoparticle depends strongly on the shape of the nanoparticle. The water density and extent of hydrogen bonding near CNT-1, particularly in the first hydration shell (see Figure 2), is significantly reduced compared to the fullerene as a result of removal of one degree of curvature. Increasing the radius of curvature of the nanotube (CNT-2 vs CNT-1) results in a further reduction in the density and extent of hydrogen bonding in the first hydration shell. Finally, for the flat graphene sheet, the water density decreases monotonically as the surface is approached, indicating the formation of a vapor−liquid-like interface between water and the graphene sheet. These results are consistent with the conventional view of hydrophobic hydration of small nonpolar solutes, which, due to a high degree of curvature, allow hydrating water to maintain a high degree of (relatively geometrically restricted) hydrogen bonding.[23−26] In the same picture, water tends to move away from extended nonpolar surfaces which interfere too severely with the ability of water to maintain hydrogen bonding, leading to increasing solvent depletion near the surface as surface curvature is reduced.

B. Realistic Nanoparticle−Water Interactions. In contrast to the dependence of the water density/free energy profiles on the shape of the nanoparticle seen for repulsive nanoparticle−water interactions, the density/free energy profiles show little dependence on the shape of the carbon nanoparticle for realistic nanoparticle−water interactions. However, the loss of water−water hydrogen bonds in the first hydration shell remains dependent on the shape of the nanoparticle, even when strong dispersion interactions exist between the carbon nanoparticle and water. The dependence of the extent of hydrogen bonding on nanoparticle shape follows the same trend observed for repulsive nanoparticle−water interactions, i.e., it decreases with decreasing nanoparticle curvature. However, a less severe reduction in the extent of hydrogen bonding is observed near nanoparticles with attractive nanoparticle−water interactions compared to that observed near nanoparticles with purely repulsive interactions with water. We believe the weaker dependence of the extent of hydrogen bonding on particle shape for nanoparticles with strong nanoparticle−water dispersion interactions is the result of the higher density of hydrating water at the nanoparticle surface compared to the same nanoparticle with repulsive interactions with water.

While the extent of water−water hydrogen bonding decreases with decreasing surface curvature, Figure 4 illustrates that the strength of the dispersion interaction of water with the carbon nanoparticles increases with decreasing surface curvature. These large offset effects result in the very similar water density/free energy profiles for the various carbon nanoparticles shown in Figure 2. Note that the strong dispersion interactions between carbon nanoparticles and water result entirely from the high density of carbon atoms on the surface of these particles. For example, we showed previously[1] that hydration of a traditional nonpolar organic solute, represented by an oil droplet the same size as a C_{60} fullerene, closely resembles that seen for repulsive C_{60}−water interactions.

IV. Water-Induced Nanoparticle−Nanoparticle Interactions

To understand how solvent-induced interactions between solutes depend on the size and shape of the solute, these interactions must be normalized in a consistent manner in order

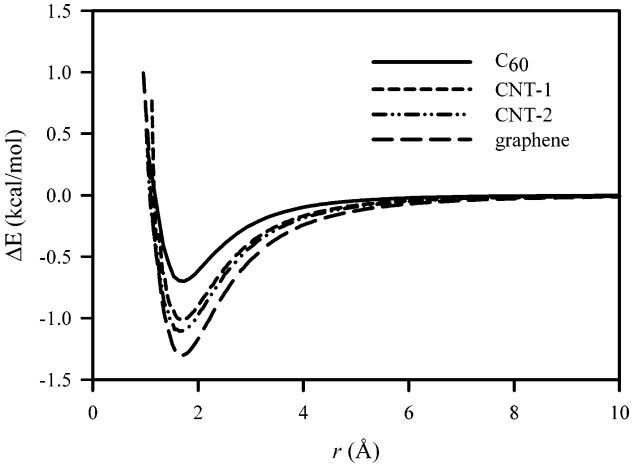

Figure 4. Potential energy profile as a single water molecule approaching a nanoparticle surface. Here *r* is measured from the surface of nanoparticle to the oxygen atom of the water molecule.

for comparisons to be meaningful. Normalization by the number of atoms per solute, the solvent-accessible surface area of the solute or the solute volume does not account for the fact that while all water molecules hydrating graphene sheets are affected when two sheets are brought together, only a fraction of the water hydrating CNTs, and an even smaller fraction of water hydrating C_{60} fullerenes, is influenced by the aggregation of two CNTs or C_{60} fullerenes. It has been reported in the literature[27] that the interaction between pairs of C_{60} fullerenes, CNTs and graphene sheets in vacuum fall on the same reduced curve, despite their geometric differences. Thus, comparison of water-induced interactions between nanoparticles of different geometries can be greatly facilitated by normalizing these interactions relative to reduced direct interactions as described below.

The PMF for the nanoparticle pairs in vacuum, shown in Figure 5a, provides the direct nanoparticle−nanoparticle interaction as a function of separation. Here the interaction is shown per sixty carbon atoms of a single particle. Carbon−carbon attraction at close nanoparticle contact (per 60 carbon atoms) increases as degrees of curvature are removed (i.e., graphene > CNT > C_{60} fullerene) since a higher fraction of the carbon atoms constituting the nanoparticle are brought into contact, increasing the depth of the nanoparticle−nanoparticle attractive well at close contact. For a fixed geometry, carbon−carbon attraction at close nanoparticle contact (per 60 carbon atoms) decreases with increasing radius of curvature (i.e., CNT-2 < CNT-1). By scaling the PMF for CNT-1, CNT-2 and graphene in vacuum (Figure 5a) by factors of 2.1, 1.6, and 10.2, respectively, the PMF as a function of separation in vacuum for all nanoparticles could be made to coincide, as shown in Figure 5b, which is consistent with the results from analytic calculations using a continuum model for the nanoparticles.[27]

The PMF for the various nanoparticle pairs in water is shown in Figure 6,[28] normalized by the factors determined from the PMF in vacuum, i.e., the PMF in water per 6.46 kcal mol^{-1} of direct interaction at nanoparticle−nanoparticle close contact. The attractive well at close contact is deep for all nanoparticles, consistent with their insolubility (aggregation) in water. The PMF for all nanoparticle pairs no longer coincide, indicating that the strength of the water-induced nanoparticle−nanoparticle interaction relative to the direct interaction depends on the shape of the nanoparticle.

The (normalized) water-induced interaction was obtained by subtracting the PMF in vacuum (Figure 5b) from that obtained

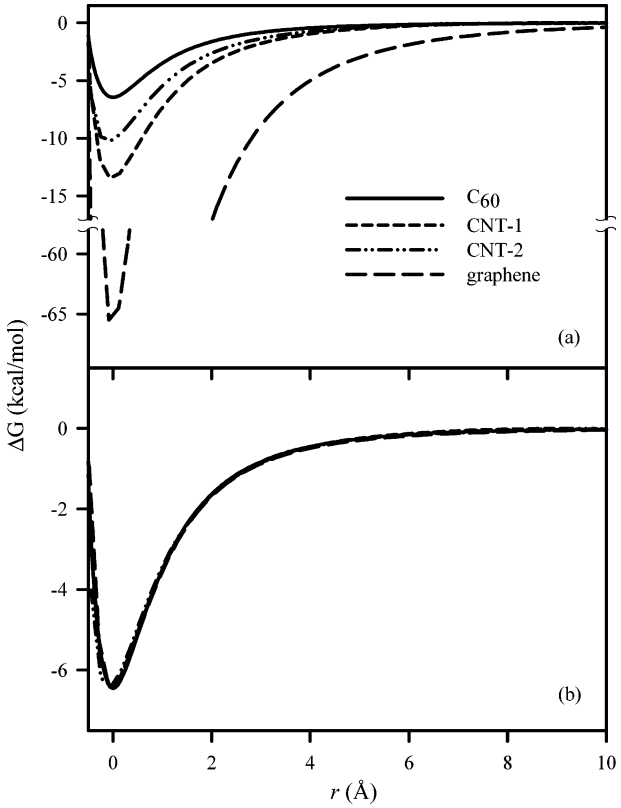

Figure 5. Nanoparticle−nanoparticle direct interaction in vacuum as a function of nanoparticle−nanoparticle surface separation (a) per sixty atoms of each nanoparticle and (b) scaled to match the minimum in the direct fullerene−fullerene interactions.

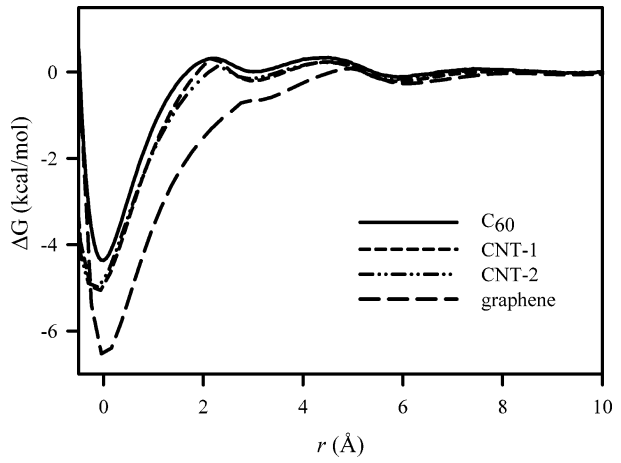

Figure 6. Potential of mean force between nanoparticle pairs in water (normalized as described in the text) as a function of nanoparticle−nanoparticle surface separation.

in water (Figure 6) and is shown in Figure 7a. As was found previously for C_{60} fullerenes,[1,2] water induces a repulsive interaction between CNTs and graphene sheets that is modulated by the structure of water. Specifically, the minima at separation of 6.0 Å and 3.3 Å correspond to two and one layer of hydrating water between the nanoparticles, respectively. Figure 7a reveals that water-induced repulsion between nanoparticles per amount of direct nanoparticle−nanoparticle interaction gained upon aggregation decreases with decreasing surface curvature; i.e., the water-induced interactions become relatively less important in the order C_{60} > CNT-1 > CNT-2 > graphene.

Table 1 shows the number of water molecules in the first hydration shell of each carbon nanoparticle per carbon atom

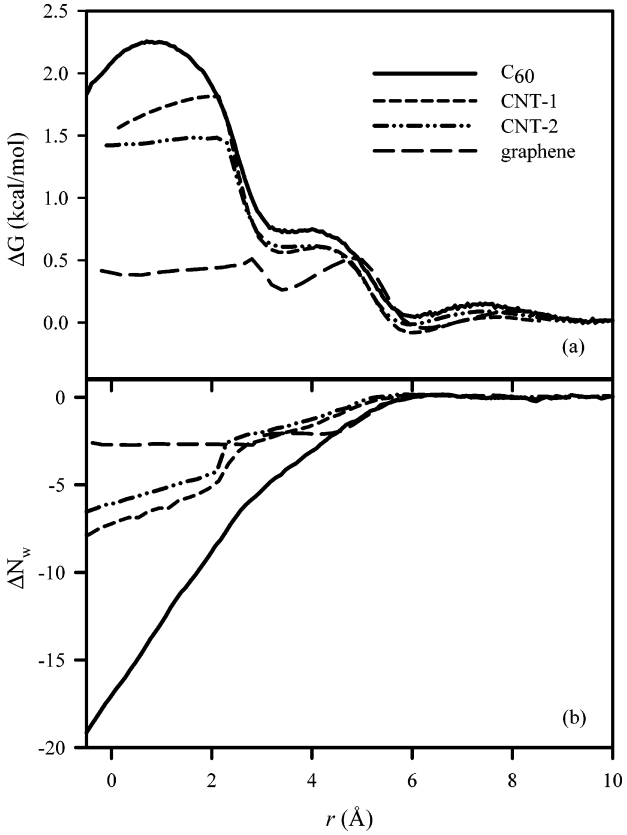

Figure 7. (a) Solvent-induced interactions between nanoparticles and (b) number of water molecules displaced from the first hydration shell of the nanoparticles (normalized as described in the text) as a function of nanoparticle−nanoparticle surface separation.

($N_{water,shell}$). $N_{water,shell}$ decreases dramatically as the curvature of the surface decreases. As a consequence, we can anticipate that the number of water molecules displaced per carbon−carbon contact created upon nanoparticle aggregation will decrease with decreasing curvature of the nanoparticle. Figure 7b shows the change in the number of water molecules in contact with the nanoparticles (within the first hydration shell) per 6.46 kcal mol^{-1} of direct interaction at contact (ΔN_w) as a function of nanoparticle separation. As anticipated, the number of water molecules displaced from the surface of the nanoparticles at close contact per amount of direct nanoparticle−nanoparticle interaction gained decreases with decreasing curvature of the nanoparticle. The free energy penalty for displacing a water molecule from the first hydration shell of a nanoparticle to the bulk can be estimated as

$$\Delta A = k_B T \ln \frac{\rho_{shell}}{\rho_{bulk}} \quad (4)$$

where ρ_{shell} is the mean density of water in the first hydration shell of a nanoparticle. Values of ρ_{shell} and ΔA as well as estimated values for the water-induced repulsion at close contact, given by

$$\Delta G_{est} = \Delta A \Delta N_w(r=0) \quad (5)$$

TABLE 2: Hydration Properties

solute	ρ_{shell} (Å^{-3})	ΔA (kcal/mol)	$\Delta N_w(r=0)$	ΔG_{est} (kcal/mol)
C_{60}	0.041	0.12	18	2.2
CNT-1	0.044	0.16	7.5	1.2
CNT-2	0.044	0.16	6.5	1.1
graphene	0.045	0.17	3	0.5

where $\Delta N_w(r=0)$ is taken from Figure 7b, are tabulated in Table 2 for each nanoparticle. ΔG_{est} agrees well with $\Delta G(r=0)$from Figure 7a, confirming that the dependence of the water-induced repulsion between nanoparticles on nanoparticle geometry arises primarily from geometry-dependent differences in the number of displaced water molecules.

Acknowledgment. The authors gratefully acknowledge NSF support through grant ITR−CHE0312226.

References and Notes

(1) Li, L.; Bedrov, D.; Smith, G. D. *Phys. Rev. E* **2005**, *71*, 011502.
(2) Li, L.; Bedrov, D.; Smith, G. D. *J. Chem. Phys.* **2005**, *123*, 204504.
(3) Wallqvist, A.; Berne, B. J. *J. Phys. Chem.* **1995**, *99*, 2893−2899.
(4) Smith, D. E.; Zhang, L.; Haymet, A. D. J. *J. Am. Chem. Soc.* **1992**, *114*, 5875−5876.
(5) Jorgensen, W. L.; Chandrasekhar, J.; Madura, J. D.; Impey, R. W.; Klei, M. *J. Chem. Phys.* **1983**, *79*, 926−935.
(6) Girifalco, L. A.; *J. Phys. Chem.* **1992**, *96*, 858−861.
(7) Cheng, A.; Klein, M. L. *Phys. Rev. Lett.* **1993**, *71*, 1200−1203
(8) Fartaria, R. P. S.; Fernandes, F. M. S. S.; Freitas, F. F. M. *J. Phys. Chem. B* **2002**, *106*, 10227−10232.
(9) Hasegawa, M.; Ohno, K. *J. Chem. Phys.* **1999**, *111*, 5955−5963.
(10) Costa, D.; Pellicane, G.; Abramo, M. C.; Caccamo, C. *J. Chem. Phys.* **2003**, *118*, 304−310.
(11) Werder, T.; Walther, J. H.; Jaffe, R. L.; Halicioglu, T.; Koumoutsakos, P. *J. Phys. Chem. B* **2003**, *107*, 1345−1352.
(12) Weeks, J. D.; Chandler, D.; Andersen, H. C. *J. Chem. Phys.* **1971**, *54*, 5237−5247.
(13) Huang, X.; Margulis, C. J.; Berne, B. J. *J. Phys. Chem. B* **2003**, *107*, 11742−11748.
(14) Walther, J. H.; Jaffe, R.; Halicioglu, T.; Koumoutsakos, P. *J. Phys. Chem. B* **2001**, *105*, 9980−9987.
(15) http://www.che.utah.edu/∼gdsmith/mdcode/main.html.
(16) Ryckaert, J. P.; Ciccotti, G.; Berendsen, H. J. C. *J. Comput. Phys.* **1977**, *23*, 327−341.
(17) Essmann, U.; Perera, L.; Berkowitz, M. L.; Darden, T.; Lee, H.; Pedersen, L. G. *J. Chem. Phys.* **1995**, *103*, 8577−8593.
(18) Frenkel, D.; Smit, B. *Understanding Molecular Simulation: From Algorithms to applications*; Academic Press: San Diego, 2002; pp 35−37.
(19) Nosé, S.; *J. Chem. Phys.* **1984**, *81*, 511−519.
(20) Hoover, W. G. *Phys. Rev. A* **1985**, *31*, 1695−1697.
(21) Anderson, H. C. *J. Chem. Phys.* **1980**, 72, 2384−2393.
(22) Tuckerman, M.; Martyna, G. J.; Berne, B. J. *J. Chem. Phys.* **1992**, *97*, 1990−2001.
(23) Lum, K.; Chandler, D.; Weeks, J. D. *J. Phys. Chem. B* **1999**, 103, 4570−4577.
(24) Huang, D. M.; Chandler, D. *J. Phys. Chem. B* **2002**, *106*, 2047−2053.
(25) Chandler, D. *Nature* **2002**, *417*, 491−491.
(26) Chandler, D. *Nature* **2005**, *437*, 640−647.
(27) Girifalco, L. A.; Hodak, M.; Lee, R. S. *Phys. Rev. B* **2000**, *62*, 13104−13110.
(28) The potential of mean force as a function of graphene−graphene separation has been adjusted to account for interaction of a graphene sheet with the water on the outside of the opposing graphene sheet. This interaction becomes important at close separations and results in a water-induced interaction between graphene sheets, even when all water between the sheets has been displaced. (Approximate) removal of this contribution to the PMF by subtracting the energetic contribution of this interaction results in a water-induced interaction that is nearly independent of graphene−graphene separation once all water molecules between the sheets are removed (Figure 7a).